Supplementary Materials for

Complex Biomineralization Pathways of the Belemnite Rostrum Cause Biased Paleotemperature Estimates

René Hoffmann *[,1], Benjamin Linzmeier [2,3], Kouki Kitajima [3], Gernot Nehrke [4], Martin Dietzel [5], Niels Jöns [1], Kevin Stevens [1] and Adrian Immenhauser [1]

[1] Ruhr-Universität Bochum, Institut für Geologie, Mineralogie und Geophysik, 44801 Bochum, North-Rhine-Westfalia, Germany; rene.hoffmann@rub.de
[2] University of South Alabama, Department of Earth Sciences, Mobile, 36688 Alabama, USA
[3] University of Wisconsin-Madison, Department of Geoscience, Madison, 53706 Wisconsin, USA
[4] Alfred Wegener Institut Helmholtz-Zentrum für Polar- und Meeresforschung, Section Marine BioGeo Sciences, 27570 Bremerhaven, Freie Hansestadt Bremen, Germany.
[5] Graz University of Technology, Institute of Applied Geosciences
* Correspondence: rene.hoffmann@rub.de

This file includes:
Extended Materials and Methods
Results and discussion of diagenetic calcite
Figure S1: Thermogravimetric analyses of different carbonate materials.
Figure S2: Classification of SIMS pits and associated $\delta^{18}O_{belemnite}$.
Figure S3: Detailed precipitation model for calcitic belemnite rostra.
Table S1: Summary statistics for the pit category data and related oxygen isotope ratios.

Materials and Methods

Materials

Here we make use of the same *Megateuthis gigantea* rostrum collected in the Nuremberg area (Bavaria, southern Germany) that was previously studied for its ultrastructure [1]. For electron microprobe analysis (EPMA) and confocal Raman spectroscopy (CRM), we used a thin section, while for SIMS analysis we used a polished thick section. The belemnite *M. gigantea* is assigned to the Middle Jurassic, early Bajocian *humphriesianum* and *garantiana* zone with a duration of 1 million years (169.7–168.7 Ma [2]. During that time, the area was located at about 34° northern latitude [3]. Based on the presence of zooxanthellate corals at the base of the *humphriesianum* zone and calcareous oolitic to primary iron oolitic deposits, the depositional setting was that of an epicontinental sea, about 60 to 80 km from the coastline, with some meters to maximal 70 m water depth within the photic zone. Detailed reconstructions of the depositional setting indicate a shallow, but fully marine environment in the tropical to subtropical zone and low sedimentation rates [4]. During the subsequent *garantiana* zone, ammonites and hexactinellid sponges occur and the sediment is bioturbated. The presence of hexactinellid sponges together with hardgrounds indicates a deeper setting below the photic zone but no deeper than 200 m, i.e. still epipelagic, as indicated by the absence of photic micro-endolithic organisms and reduced sediment input [5,6].

The good preservation of belemnite rostra is indicated by the presence of an intact fibrous microfabric in combination with cathodoluminescence as is commonly used to identify well-preserved belemnite rostra [7,8]. The dark blue to bluish, intrinsic luminescence (pure stoichiometric calcite), and the lack of cloudy areas, exfoliation, abundant fracture and microstylolites or boring traces support the interpretation of a well-preserved rostrum calcite [9].

Methods

Thermogravimetric analysis (TGA) allows determining the content of volatile components like water and organic molecules within biogenic carbonates [10]. Analyses were performed using a Mettler Toledo TGA/DSC 1. Approximately, 15 mg of powder was obtained by milling using a high-precision drill (Minimo C121; Minitor Co., Ltd, Alfred Wegener Institut Helmholtz-Zentrum für Polar- und Meeresforschung, Section Marine BioGeoSciences) with a 1 mm cylindrical bit (Komet/Gebr. Brasseler GmbH and Co. KG, Alfred Wegener Institut Helmholtz-Zentrum für Polar- und Meeresforschung, Section Marine BioGeoSciences) attached on a binocular microscope. The measurements were performed using 70 µl alumina crucibles closed with an alumina lid having a hole of ~1 mm. The gas flow was set to 20 ml min^{-1} N_2 and the heating rate set to 10 K min^{-1}. Results from the belemnite calcite were compared with data from inorganic natural calcite (Iceland spar), an organic-rich stalagmite [11], and an organic-rich coral skeleton bleached in hydrogen peroxide before analysis. This was done in order to assess the influence of organic matter on conventional stable isotope analysis and SIMS analysis (see below, Figure S1).

Raman imaging was performed using a WITec alpha 300 R (WITec GmbH, Alfred Wegener Institut Helmholtz-Zentrum für Polar- und Meeresforschung, Section Marine BioGeoSciences) confocal Raman microscope. The scan was performed using a piezoelectric scanner table having a minimum step size of 4 nm. The scan area was chosen to be 150 µm × 150 µm and 600 points per line and 600 lines was the resolution chosen with an integration time of 0.2 s per spectrum. The excitation wavelength was 488 nm and an ultra-high throughput spectrometer (UHTS 300, WITec, Alfred Wegener Institut Helmholtz-Zentrum für Polar- und Meeresforschung, Section Marine BioGeoSciences) was used. The spectrometer was set to a grating, 600/mm, 500 nm blaze and the used lens was a Nikon MPlan FL N 100× (Alfred Wegener Institut Helmholtz-Zentrum für Polar- und Meeresforschung, Section Marine BioGeoSciences) with an NA of 0.90. Data analysis was done by means of the WITec Project FOUR 4.0 software (Alfred Wegener Institut Helmholtz-Zentrum für Polar- und Meeresforschung, Section Marine BioGeoSciences). The dedicated Raman bands within a Raman spectrum allow the identification of many organic and inorganic compounds. However, even if no dedicated Raman band appear in a Raman spectrum, an enhanced background fluorescence has been shown to be indicative for the presence of diagenetically altered organic compounds [12,13].

The elemental composition of the sample was determined using a field-emission electron microprobe (EMP) Cameca SXFiveFE (central microanalytical laboratories, Ruhr-Universität Bochum). The instrument is equipped with five wavelength-dispersive spectrometers and an energy-dispersive SDD system. Quantitative analyses were done *in situ* in a polished and 10–15 nm thick carbon-coated thin section. An acceleration voltage of 15 kV and a probe current of 10 nA were used. As carbonate is very beam sensitive, a defocused beam (5 µm) was used and time-dependent X-ray intensity changes were taken into account. For quantification of the data we used the X-Phi correction procedure [14]. For Ca, Mg, and Sr the Smithsonian carbonate microbeam standards were used [15,16]. Further standards were natural apatite for P, and celestine for S.

Due to beam sensitivity and low elemental concentrations in the sample, X-ray element mapping required special attention. Intensive testing with different acceleration voltages, conductive coatings, beam currents and dwell times was necessary to obtain a satisfactory result. We used an acceleration voltage of 8 kV that facilitated collection of a high spatial resolution image. However, to obtain reasonable X-ray count rates, a beam current of ca. 400 nA and a dwell time of 75 ms per pixel were chosen. Compared to a 10–15 nm thick carbon-coated sample, better results were achieved using 10 nm conductive gold coating for mapping. Although X-ray absorption is higher using gold coating, the improved thermal conductivity prevented sample damage at these extreme analytical conditions.

Secondary Ion Mass Spectroscopy (SIMS) allowing for *in situ* stable isotope analysis was performed using the CAMECA IMS 1280 ion microprobe (WiscSIMS, Department of Geoscience, University of Wisconsin). High-precision (0.3‰, 2 standard deviation) analyses of $\delta^{18}O$ with an approximately 10 μm diameter ion beam that excavate pits 1 μm deep are measured in carbonates [17–20]. Analysis of the belemnite was done with a standard-sample-standard bracketing technique, using two brackets of four analyses of UWC-3 ($\delta^{18}O$ = −17.87‰, Vienna Pee Dee Belemnite, VPDB [17]. Each analysis was positioned based on backscattered electron and reflected light images. Analysis pits were imaged with a scanning electron microscope (SEM) and transmitted light and classified. QGIS-maps [21] of compiled SEM images of the sample surface including SIMS analysis pit images are included as supplemental data (Figure S2).

It is important to weigh the possibility that measured $\delta^{18}O$ differences between CP1, CP2, and LDC are caused by factors inherent in the SIMS analysis. Our quantitative EPMA results indicate differences of only ~1000 $\mu g\ g^{-1}$ for Mg and Sr (highest for each element <2500 $\mu g\ g^{-1}$) between the different types of calcite. Such a small difference in minor element chemistry has not been shown to influence SIMS-measured $\delta^{18}O$ in carbonates [22]. There is a detectable, qualitative difference in the amount of organic matter visualized by CRM (Fig. 1E). TGA analyses revealed a total weight loss of about 1% with a weight loss of 0.4% between 0–200 °C attributed to water loss, while weight loss between 200–600 °C is attributed to the combustion of organic matter [10]. Above 600 °C decomposition of $CaCO_3$ into CaO begins [23]. Such small differences in quantities of organic matter within a speleothem [24] and a *Nautilus* shell [18] did not appear to alter $\delta^{18}O$ values. Similarly, a negligible effect of the organic compounds in the belemnite calcite on the $\delta^{18}O$ values is assumed.

A single bulk powder sample was taken from a trench parallel and within 3 mm of the microanalytical transect for bulk stable isotope analysis. The $\delta^{18}O$ and $\delta^{13}C$ were measured by gas source mass spectrometry at Northwestern University using a Thermo Scientific Delta V Plus isotope ratio mass spectrometer attached to a Thermo Gasbench II/CTC GC-PAL autosampler. Precision for $\delta^{18}O$ is ±0.22‰ and for $\delta^{13}C$ is ±0.06‰. Powder was reacted with orthophosphoric acid in a Helium flushed vial and the resulting gas was measured. Analyses were calibrated against NBS-18 (carbonatite) and NBS-19 (calcite) standards. Measured $\delta^{18}O$ by this method is +1.0‰ relative to average SIMS measured $\delta^{18}O$ for all material in this study, but is within analytical uncertainty of the mean of CP2 that composes 50–90% of the rostrum. Similar patterns of offset in techniques have been observed in other low-temperature carbonates including foraminifera [25], speleothems [26], and otoliths [27,28], although this offset has not been observed in high temperature carbonates [29].

For relative temperature reconstruction we used the temperature coefficient from [30]. The temperature to $\delta^{18}O$ slopes are statistically indistinguishable across the carbonate phases and experiments discussed by Kim et al. [30]. Because we calculate the range of temperatures using the slope coefficient given the measured $\delta^{18}O$ rather than a specific paleotemperature, the estimated high range of temperatures is robust to the choice of equation. We estimate this range to be about 16 °C.

Supplementary Text

Late diagenetic calcite (LDC)

Absence of fluorescence in CRM-images (Figure 1E) characterized the LDC as composed of pure calcite (lack of enhanced fluorescence from organic matter). The LDC is further characterized by the lowest concentrations of Sr, Mg, S, and P, i.e. it is nearly stoichiometric calcite. SIMS analyses on this type of calcite have given a $\delta^{18}O$ value that is on average −2.1‰ (VPDB, n = 4), a value much lower than the other two calcite phases (Figure 2).

The morphology of areas composed of LDC suggests they are former open cracks filled with late diagenetic calcite (Figure 1E). This non-biological controlled calcite forms a minor portion in many geochemically analyzed rostra. Due to the higher amounts of

manganese such late diagenetic portions of belemnite rostra can be easily identified using the cathodoluminescence microscope [1]. Although, LDC often shows a bright orange luminescence in CL images, the amounts of Mn and Fe are close to or below the detection limits of the electron microprobe.

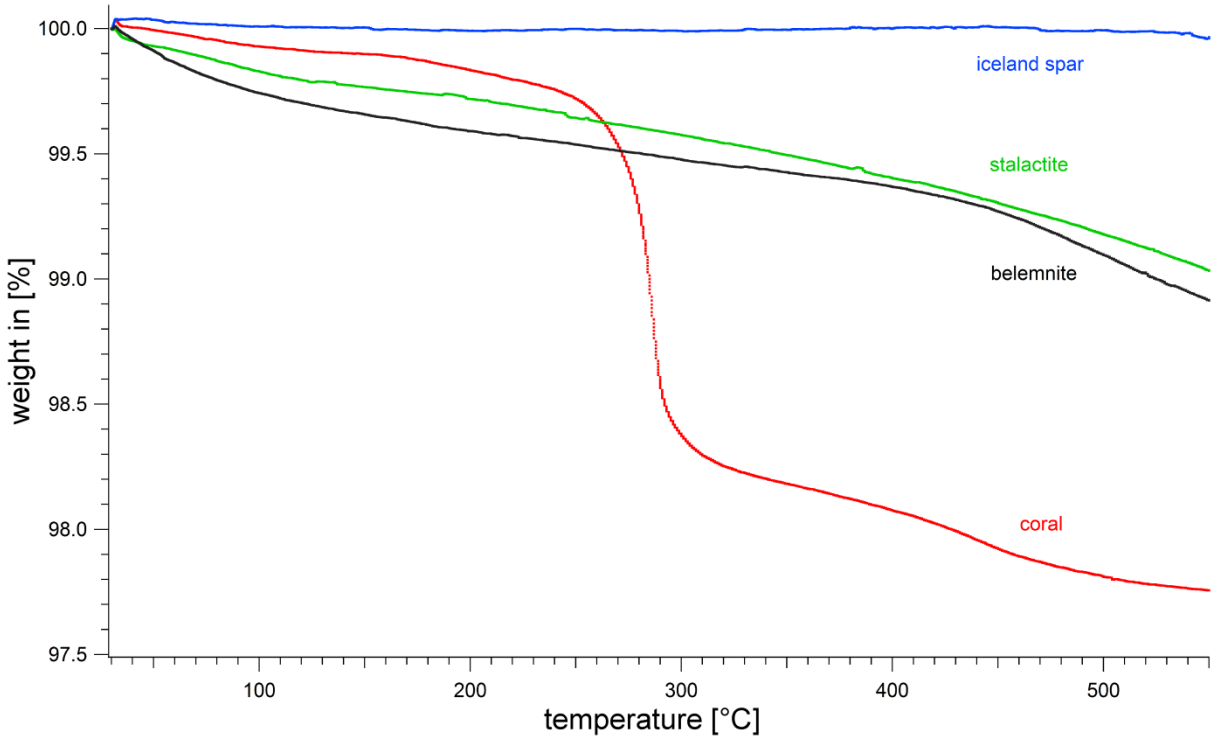

Figure S1. Thermogravimetric analyses of different carbonate materials. Comparing the organic lean Iceland spar with nearly no weight loss, with an organic rich stalagmite, belemnite calcite and corals skeleton. Note the similar amount and course of weight loss between the stalagmite and the belemnite carbonate, while the coral shows the highest amount of weight loss presumable due to the presence of higher amounts of organic material in the coral skeleton. Note that the coral skeleton loses less weight between 0–200 °C, i.e. presumably contains less water than the belemnite. Above 200 °C the weight loss quickly exceeds that of the belemnite calcite suggesting higher amounts of organic matter in the coral skeleton.

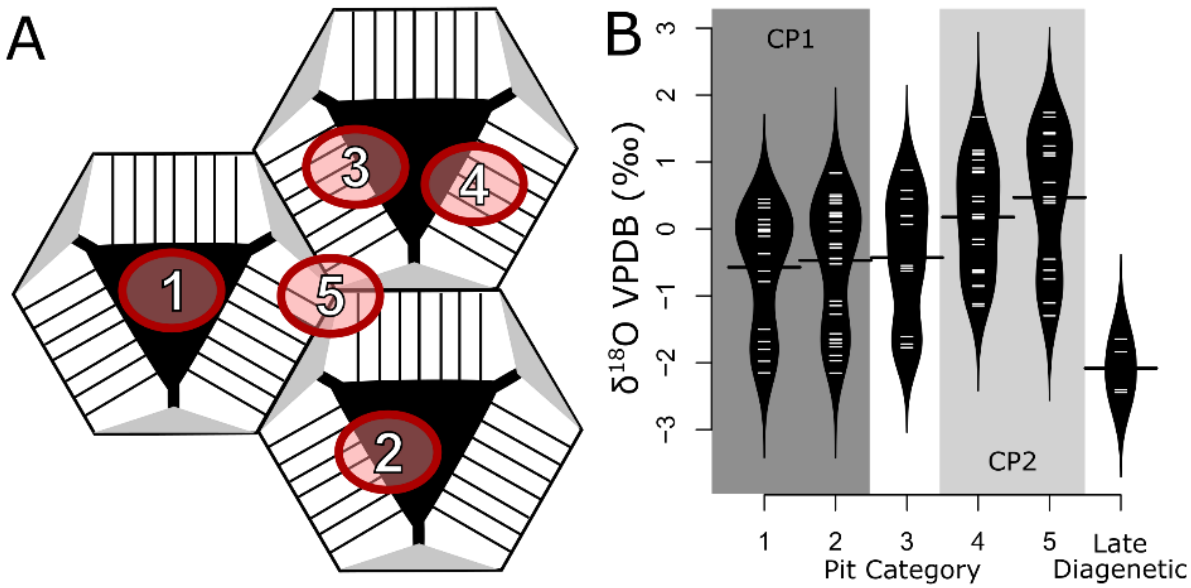

Figure S2. Classification of SIMS pits and associated $\delta^{18}O_{belemnite}$. (**A**), Pits produced during SIMS oxygen isotope analysis were classified according to their position relative to the biologically controlled (CP1) or biologically induced (CP2) calcite phases: 1 = 100% in CP1, 2 = 75% in CP1 and 25% in CP2, 3 = 50% in the first and 50% in the second calcite phases, 4 = 25% in the first and 75% in the second calcite phases, and 5 = 0% in the first and 100% in the second calcite phases (CP2). (**B**), Beanplot [31] showing SIMS measured $\delta^{18}O_{belemnite}$ values are generally higher in the second calcite phase.

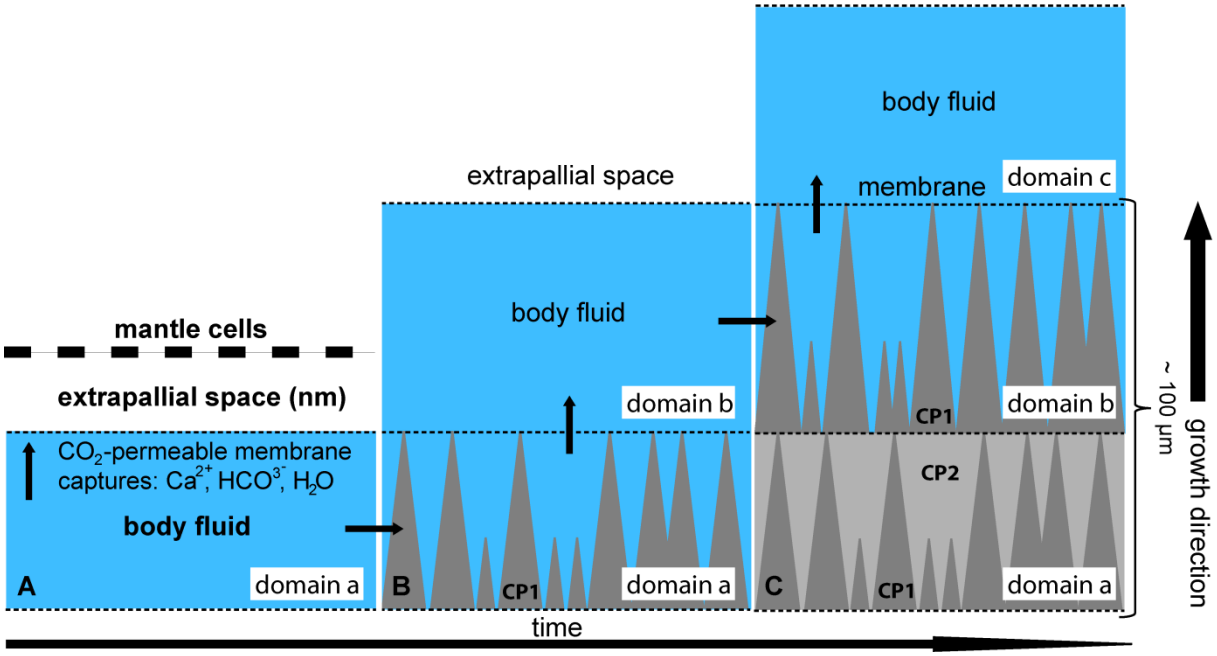

Figure S3. Detailed precipitation model for calcitic belemnite rostra. (**A**) Mantle cells secrete organic membranes that are more or less equidistant (a few nanometers) and confine a distinct space filled with body fluids. The membranes are CO_2-permeable but capture Ca^{2+}, HCO^{3-}, and H_2O and contain the enzyme carbonic anhydrase ([32–34]. (**B**) Within the confined space (domain a), secretion of a single layer of trigonal pyramids within an organic scaffold framework starts. Those trigonal pyramids, representing CP1, form the belemnite skeleton—a highly porous, organic-rich, filigree framework, with their tips pointing towards to the surface of the rostrum. The primary pore space was filled with the remains of the body fluid but altered pH and geochemical composition. In a next step a new membrane forms confining a new fluid filled space (domain b), (**C**) The second generation of trigonal pyramids was secreted in domain b. During the second or third pyramid formation cycle the pore space of the first pyramid generation in domain a becomes occluded by isopachous, organic-lean, calcite cements (CP2). The occlusion of the pore space results in a dense fabric composed of two distinct calcite phases (CP1 and CP2), that differ in the timing of formation, geochemical composition, and the formation process.

Table S1. Summary statistics for the pit category data and related oxygen isotope ratios.

Pit Class	Mean $\delta^{18}O$ (‰ VPDB)	2 SD $\delta^{18}O$ (‰)	Number of Analyses	Lowest $\delta^{18}O$ (‰ VPDB)	Highest $\delta^{18}O$ (‰ VPDB)
1-CP1	−0.6	1.8	17	−2.2	0.4
2-CP1	−0.5	1.9	32	−2.2	0.8
3	−0.4	1.9	11	−1.8	0.9
4-CP2	0.2	1.7	23	−1.2	1.7
5-CP2	0.5	2.0	16	−1.3	1.7
LDC	−2.1	0.8	4	−2.4	−1.6

References

1. Hoffmann, R.; Richter, D.K.; Neuser, R.D.; Jöns, N.; Linzmeier, B.J.; Lemanis, R.E.; Fusseis, F.; Xiao, X.; Immenhauser, A. Evidence for a composite organic–inorganic fabric of belemnite rostra. Implications for palaeoceanography and palaeoecology. *Sed. Geol*. **2016**, *341*, 203–215.
2. Gradstein, F.M.; Ogg, J.G.; Schmitz, M.; Ogg, G. (Eds.) *The Geologic Time Scale* **2012**; 2-Volume Set; Elsevier: Amsterdam, The Netherlands, 2012; 1176p.
3. Hinsbergen, D.J.J.; van Groot, L.V.; de Schaik, S.J.; van Spakman, W.; Bijl, P.K.; Sluijs, A.; Langereis, C.G.; Brinkhuis, H. A Paleolatitude Calculator for Paleoclimate Studies. *PLoS ONE* **2015**, *10*, e0126946.

4. Anagnōstu, C. Sedimentpetrographische Untersuchungen im Mittleren und Oberen Dogger Süddeutschlands. Ph.D.Thesis, *Boch. Geol. Geotech. Arb.* **1987**, *25*, 1–291.
5. Arp, G. Fazies, Stratigraphie und Ammonitenfauna des Mittleren und Oberen Dogger bei Neumarkt id Opf. (Bajocium-Oxfordium, Süddeutschland). *Berl. Geowiss. Abh. E* **2001**, *36*, 189–241.
6. Wetzel, A.; Weissert, H.; Schaub, M.; Voegelin, A.R. Sea-water circulation on an oolite-dominated carbonate system in an epeiric sea (Middle Jurassic, Switzerland). *Sedimentology* **2013**, *60*, 19–35.
7. Rosales, I.; Quesada, S.; Robles, S. Primary and diagenetic isotopic signals in fossils and hemipelagic carbonates: The Lower Jurassic of northern Spain. *Sedimentology* **2001**, *48*, 1149–1169.
8. Ullmann, C.V.; Korte, C. Diagenetic alteration in low-Mg calcite from macrofossils: A review. *Geol. Q.* **2015**, *59*, 3–20.
9. Sælen, G. Diagenesis and construction of the belemnite rostrum. *Palaeontology* **1989**, *32*, 765–798.
10. Cuif, J.-P.; Dauphin, Y.; Berthet, P.; Jegoudez, J. Associated water and organic compounds in coral skeletons: Quantitative thermogravimetry coupled to infrared absorption spectrometry. *Geochem. Geophys.* **2004**, *5*, Q11011.
11. Pacton, M.; Breitenbach, S.F.M.; Lechleitner, F.A.; Vaks, A.; Rollion-Bard, C.; Gutareva, O.S.; Osintcev, A.V.; Vasconcelos, C. The role of microorganisms in the formation of a stalactite in Botovskaya Cave, Siberia paleoenvironmental implications. *Biogeosciences* **2013**, *10*, 6115.
12. Nehrke, G.; Nouet, J. Confocal Raman microscope mapping as a tool to describe different mineral and organic phases at high spatial resolution within marine biogenic carbonates: Case study on *Nerita undata* (Gastropoda, Neritopsina). *Biogeosciences* **2011**, *8*, 3761–3769.
13. Wall, M.; Nehrke, G. Reconstructing skeletal fiber arrangement and growth mode in the coral *Porites lutea* (Cnidaria, Scleractinia): A confocal Raman microscopy study. *Biogeosciences* **2012**, *9*, 4885–4895.
14. Merlet, C. An accurate computer correction program for quantitative electron probe microanalysis. *Microchim. Acta* **1994**, *114–115*, 363–376.
15. Jarosewich, E.; MacIntyre, I.G. Carbonate reference samples for electron microprobe and scanning electron microscope analyses. *J. Sediment. Res.* **1983**, *53*, 677–678.
16. Jarosewich, E.; White, J.S. Strontianite reference sample for electron microprobe and SEM analyses. *J. Sediment. Res.* **1987**, *57*, 762–763.
17. Kozdon, R.; Ushikubo, T.; Kita, N.T.; Spicuzza, M.; Valley, J.W. Intratest oxygen isotope variability in the planktonic foraminifer *N. pachyderma*: Real vs. apparent vital effects by ion microprobe. *Chem. Geol.* **2009**, *258*, 327–337.
18. Linzmeier, B.J.; Kozdon, R.; Peters, S.E.; Valley, J.W. Oxygen isotope variability within *Nautilus* shell growth bands. *PLoS ONE* **2016**, *11*, e0153890.
19. Śliwiński, M.G.; Kitajima, K.; Kozdon, R.; Spicuzza, M.J.; Fournelle, J.H.; Denny, A.; Valley, J.W. Secondary Ion Mass Spectrometry Bias on Isotope Ratios in Dolomite–Ankerite, Part II: $\delta^{13}C$ Matrix Effects. *Geostand. Geoanalytical Res.* **2016**, *40*, 173–184.
20. Denny, A.C.; Kozdon, R.; Kitajima, K.; Valley, J.W. Isotopically zoned carbonate cements in Early Paleozoic sandstones of the Illinois Basin: $\delta^{18}O$ and $\delta^{13}C$ records of burial and fluid flow. *Sed. Geol.* **2017**, *361*, 93–110.
21. Linzmeier, B.J.; Kitajima, K.; Denny, A.C.; Cammack, J.N. Making maps on a micrometer scale. *Eos* **2018**, *99*, doi:10.1029/2018EO099269.
22. Śliwiński, M.G.; Kitajima, K.; Kozdon, R.; Spicuzza, M.J.; Fournelle, J.H.; Denny, A.; Valley, J.W. Secondary Ion Mass Spectrometry Bias on Isotope Ratios in Dolomite–Ankerite, Part I: $\delta^{18}O$ Matrix Effects. *Geostand. Geoanalytical Res.* **2016**, *40*, 157–172.
23. Checa, A.G.; Macías-Sánchez, E.; Harper, E.M.; Cartwright, J.H.E. Organic membranes determine the pattern of the columnar prismatic layer of mollusc shells. *Proc. R. Soc. B* **2016**, *283*, 20160032.
24. Orland, I.J.; Bar-Matthews, M.; Ayalon, A.; Matthews, A.; Kozdon, R.; Ushikubo, T.; Valley, J.W. Seasonal resolution of Eastern Mediterranean climate change since 34 ka from a Soreq Cave speleothem. *Geochim. Cosmochim. Acta* **2012**, *89*, 240–255.
25. Wycech, J.B.; Kelly, D.C.; Kozdon, R.; Orland, I.J.; Spero, H.J.; Valley, J.W. Comparison of $\delta^{18}O$ analyses on individual planktic foraminifer (*Orbulina universa*) shells by SIMS and gas-source mass spectrometry. *Chem. Geol.* **2018**, *483*, 119–130.
26. Orland, I.J.; Edwards, R.L.; Cheng, H.; Kozdon, R.; Cross, M.; Valley, J.W. Direct measurements of deglacial monsoon strength in a Chinese stalagmite. *Geology* **2015**, *43*, 555–558.
27. Aubert, M.; Williams, I.S.; Boljkovac, K.; Moffat, I.; Moncel, M.-H.; Dufour, E.; Grün, R. In situ oxygen isotope micro-analysis of faunal material and human teeth using a SHRIMP II: A new tool for palaeo-ecology and archaeology. *J. Archaeol. Sci.* **2012**, *39*, 3184–3194.
28. Helser, T.E.; Kastelle, C.R.; McKay, J.L.; Orland, I.J.; Kozdon, R.; Valley, J.W. Evaluation of micromilling/conventional isotope ratio mass spectrometry and secondary ion mass spectrometry of $\delta^{18}O$ values in fish otoliths for sclerochronology. *Rapid Commun. Mass Spectrom.* **2018**, *32*, 1781–1790.
29. Ferry, J.M.; Ushikubo, T.; Kita, N.T.; Valley, J.W. Assessment of grain-scale homogeneity and equilibration of carbon and oxygen isotope compositions of minerals in carbonate-bearing metamorphic rocks by ion microprobe. *Geochim. Cosmochim. Acta* **2010**, *74*, 6517–6540.
30. Kim, S.-T.; O'Neil, J.R.; Hillaire-Marcel, C.; Mucci, A. Oxygen isotope fractionation between synthetic aragonite and water: Influence of temperature and Mg2+ concentration. *Geochim. Cosmochim. Acta* **2007**, *71*, 4704–4715.
31. Kampstra, M.P. Package 'Beanplot'. 2014. Available online: http://cran-mirror.cs.uu.nl/web/packages/beanplot/beanplot.pdf (accessed on 09 December 2015).
32. Miyamoto, H.; Miyashita, T.; Okushima, M.; Nakano, S.; Morita, T.; Matsushiro, A. A carbonic anhydrase from the nacreous layer in oyster pearls. *Proc. Natl. Acad. Sci. USA* **1996**, *93*, 9657–9660.
33. McConnaughey, T.A. Sub-equilibrium oxygen-18 and carbon-13 levels in biological carbonates: Carbonate and kinetic models.

Coral Reefs **2003**, *22*, 316–327.
34. Uchikawa, J.; Zeebe, R.E. The effect of carbonic anhydrase on the kinetics and equilibrium of the oxygen isotope exchange in the CO_2–H_2O system: Implications for $\delta^{18}O$ vital effects in biogenic carbonates. *Geochim. Cosmochim. Acta* **2012**, *95*, 15–34.